Modification on the chloride binding capacity of alkali activated slag by applying calcium and aluminium containing phases

Yang, Tingli; Fan, Xiaochun; Gao, Xu; Gu, Qian; Xu, Shi; Shui, Zhonghe

DOI
10.1016/j.conbuildmat.2022.129427

Publication date
2022

Document Version
Final published version

Published in
Construction and Building Materials

Construction and Building Materials 358 (2022) 129427

Contents lists available at ScienceDirect

Construction and Building Materials

journal homepage: www.elsevier.com/locate/conbuildmat

Modification on the chloride binding capacity of alkali activated slag by applying calcium and aluminium containing phases

Tingli Yang [a], Xiaochun Fan [a], Xu Gao [a,*], Qian Gu [a,*], Shi Xu [b,d], Zhonghe Shui [c]

[a] School of Civil Engineering and Architecture, Wuhan University of Technology, Wuhan 430070, China
[b] Hubei Key Laboratory of Roadway Bridge and Structure Engineering, Wuhan University of Technology, Wuhan 430070, China
[c] State Key Laboratory of Silicate Materials for Architectures, Wuhan University of Technology, Wuhan 430070, China
[d] Civil Engineering and Geosciences, Delft University of Technology, 2628CN Delft, the Netherlands

ARTICLE INFO

Keywords:
Alkali-activated materials
Chloride binding capacity
Hydration products
Friedel's salt
Thermodynamic modelling

ABSTRACT

In this study, a modified alkali activated slag system is designed by introducing additional calcium and aluminum containing phases in the binder, aiming at promote the formation of Friedel's salt (Fs) within the reaction products and therefore achieve a better chloride binding capacity. The effect of calcium and alumina contents on phase composition, chloride binding behavior, pore structure and mechanical properties of alkali activated slag are investigated. The results show that the addition of $Ca(OH)_2$ and nano γ-Al_2O_3 (CH and NA) results in the residual CH within the reaction products, but when in present of chloride, all residual CH transformed into Fs or other phases. The chloride binding capacity of the binder is obviously enhanced by CH and NA addition, owing to the increased ability to chemically bind chloride through Fs formation. There also exists an optimum Ca/Al ratio of the starting material regarding the chloride binding capacity. Adding CH coarsen the pore structure of the hydrated matrix by increase the amount of pores with the sizes larger than 200 nm, while NA exhibits a contrary effect. The chloride chemically binding behavior, namely the formation of Fs, slightly reduced the porosity of the binder. The strength results illustrate the negative effect of CH on compressive strength, and NA presents a positive effect, the modified binding system is able to provide a comparable mechanical property when compared with the reference alkali activated mixture.

1. Introduction

Alkali activated material are sustainable substitute of ordinary Portland cement that are natural or artificial aluminosilicates activated by hydroxide-, silicate- or alkaline carbonate-solutions [1,2]. Commonly applied raw materials for alkali activation include natural minerals or industrial by-products such as fly ash, slags, metakaolin and nature pozzolans [3–5]. The main reaction product after activation are calcium aluminosilicate hydrate (C-A-S-H) or alkali aluminosilicate (*N*-A-S-H) type gels depending on the reaction mechanisms, and secondary phases of hydrotalcite, zeolite and AFm type phases are sometimes presented [6,7]. Compared to ordinary Portland cement, alkali activated materials show advantages in energy consumption and carbon emission [8,9], as well as better mechanical properties, resistance to penetration and other durability related issues [1,10,11].

On the other hand, as the increasing demand of developing marine areas, the durability design of infrastructure served in marine environment has attracted great attention. The harsh marine environment usually results in an faster deterioration of concrete structures, mainly by free chloride induced rusting of embedded steels [12,13]. Given this, researches have been done on preventing the chloride induced corrosion, and it is generally agreed that a better resistance to chloride attack can be effectively achieved by refining the pore structure or increasing the chloride binding capacity of the binder [14–16]. As a high performance binding material with intrinsic low porosity, alkali activated material also exhibits the potential to be applied in marine environment for the durability concern.

Regarding the chloride binding behaviors, there are two types of bound chlorides in hydrated matrix [17], one is the physically bound chloride that owning to the physical adsorption of chloride by the hydrated C-S-H type gels, the other is the chemically bound one that due to the chemical reaction between chloride, calcium and alumina phases to form chloroaluminates such as Friedel's salt [18–20]. In Portland cement system, large amount of research has verified the importance of

* Corresponding authors.
E-mail address: x.gao@whut.edu.cn (X. Gao).

https://doi.org/10.1016/j.conbuildmat.2022.129427
Received 7 December 2021; Received in revised form 5 October 2022; Accepted 10 October 2022
Available online 20 October 2022

alumina enriched supplementary cementitious materials (SCMs) in improving the chloride binding capacity, because the additionally provided aluminate in SCMs can react with calcium hydroxide to form Friedel's salt, therefore more free chlorides can be chemically bound [21–23]. Whilst in alkali activated system, factors affecting the chloride binding behavior were also investigated. Provis found that similar to Portland cement system, the AFm type phases (precursor of Freidel's salt) is still the most effective chloride chemically binding phase in alkali activated system [24]. The study of Shi showed that in alkali activated systems, the Freidel's salt only present in alkali activated high calcium binders after chloride attack, namely not formed in geopolymers, indicating the importance of calcium content [25]. Mangat found that the amount of Freidel's salt in reaction products of alkali activated slag is affected by the Ca/Al and Ca/Si ratios of the starting materials [26], similar result was also observed in a study on the chloride binding capacity of lime-SCM binding systems [27]. Zhu studied the phase assemblage of alkali activated slag when calcium hydroxide was incorporated, an significant increase of C_2ASH_8 and C_4AH_{13} content within the reaction products was identified [28], the presence of those AFm type phases may demonstrate a better chloride binding capacity of the binder [29]. Previous researches have shown a preliminary indication that promoting the formation of Friedel's salt in presence of chloride can be an ideal approach to improve the chloride binding capacity of alkali activated materials, and this capacity may closely related to the chemical composition of the binder, especially the content of calcium and aluminum. However at current state, raw materials are often directly mixed with activator to produce alkali activated binders, limited attention was paid to tailor the binder composition for a certain property of alkali activated materials.

In this study, a modified alkali activated binding system is designed, blast furnace slag is used as the main binding precursors, additional calcium and alumina phases are used together to adjust the chemical composition of the starting material, aiming at achieving a better chloride binding capacity of the binder. The effect of starting materials, especially the calcium and alumina content, on phase composition, chloride binding behavior, pore characteristics and mechanical properties of alkali activated slag are discussed in detail, principles of optimizing the chloride binding capacity of alkali activated slag are suggested.

2. Experimental

2.1. Materials

The binding material used in this study was a commercial ground granulated blast furnace slag (GBFS), type P·I grade 42.5 Portland cement (OPC) was also used as a reference binder. Commercial water glass (22.8 % SiO_2, 16.8 % Na_2O and 60.4 % H_2O by weight, respectively) and analytical grade sodium hydroxide were used to produce alkali activator with a target modulus. As for the phase adjusting materials, analytical grade calcium hydroxide (CH) pellets was used as additional calcium source, while gamma-phase nano alumina slurry (NA, 20 % Al_2O_3 and 80 % H_2O) was selected as alumina adjusting phases. Deionized water was used in order to achieve proper water to binder ratios of the paste mixtures. The major chemical composition of applied starting materials is listed in Table 1.

2.2. Mix proportions

The mix proportions used in this study are listed in Table 2. All mixtures share a fixed water to binder ratio of 0.48 and an equivalent Na_2O content of 5 % by mass of the binder, based on previous experiences of the authors [30,31]. A water glass solution with a modulus of 1.4 (molar ratio of SiO_2 to Na_2O) was produced by mixing commercial water glass solutions with appropriate amount of sodium hydroxide. The ordinary Portland cement paste is prepared as a reference. Regarding the alkali activated mixtures, according to the preliminary thermodynamic simulation and basic tests of fluidity and mechanical properties results, a fixed replacement of slag by 15 wt% is applied in alkali activated mixtures, and four levels of γ-Al_2O_3 replacements (1 %, 3 %, 5 % and 7 %) by mass are used, therefore the corresponding $Ca(OH)_2$ contents in each mix is 14 %, 12 %, 10 % and 8 %, respectively. All samples are prepared in plastic molds of 40 mm × 40 mm × 40 mm for compressive strength [32,33], then demolded after 1d of curing, and then cured at a temperature of 20 °C and a relative humidity of 95 % until testing. Additionally, the experiment process of this study is illustrated in Fig. 1.

2.3. Testing methods

The phase assemblage of mixtures before and after exposing to chloride solution was identified by X-ray diffraction and thermogravimetry analysis. The XRD analysis was carried out using a Cu target, with 0.02° per step size and 10 ~ 80° scan range by a Ultima Ⅳ X-ray diffractometer. The thermal analysis (TG/DTG) was conducted by using a STA449F3 instrument, and samples were heated up to 1000 °C at a rate of 10 °C/min with nitrogen as the carrier gas.

The bound chloride content was measured through the equilibrium method proposed by Tang and Nilsson [34]. The hardened pastes were grounded and dried in a vacuum oven at 50 °C until a constant weight. Then 6 g of the sample and 30 ml of 0.5 M NaCl solution were added in a 50 ml vial, and shaken to homogenize after tightly capped. The bound chloride content after 1 month of chloride immersion was determined by titrating the filtrate with $AgNO_3$ solution. The calculation method is shown in Formula (1), and the final result of each sample is the average of 3 parallel tests.

$$m_c = \frac{M_{Cl}}{m_i}\cdot\left(C_i \cdot V_i - 60 \cdot C_{Ag} \cdot V_{Ag}\right) \quad (1)$$

where, m_c is the total bound chloride per gram of hydrated cement blend, mg/g; M_{cl} is the molar mass of chloride, 35.45 g/mol; m_i is the mass of the sample powder exposed to the chloride salt solution, 6 g; C_i is the concentration of initial chloride salt solution, 0.5 mol/L; V_i is the volume of exposure solution, 30 ml; C_{Ag} is the concentration of $AgNO_3$ solution, 0.02 mol/L; V_{Ag} is the consumption of $AgNO_3$ solution, mL.

According to the method proposed by Shi and Geiker [20], the

Table 2
Mix proportions.

Sample ID	Na_2O	M_s	OPC	Slag	γ-Al_2O_3	$Ca(OH)_2$	W/B
OPC	–	–	100 %	–	–	–	0.48
S0	5 %	1.4	–	100 %	0	0	0.48
SCA1	5 %	1.4	–	85 %	1 %	14 %	0.48
SCA2	5 %	1.4	–	85 %	3 %	12 %	0.48
SCA3	5 %	1.4	–	85 %	5 %	10 %	0.48
SCA4	5 %	1.4	–	85 %	7 %	8 %	0.48

Table 1
Major chemical composition of the binding materials.

Materials	CaO	SiO_2	Al_2O_3	Fe_2O_3	MgO	Na_2O	K_2O	SO_3	LOI
GBFS	41.10	31.32	14.45	0.33	6.91	0.27	0.35	3.99	1.28
OPC	56.74	23.46	6.51	3.18	2.33	0.20	0.87	2.44	4.27

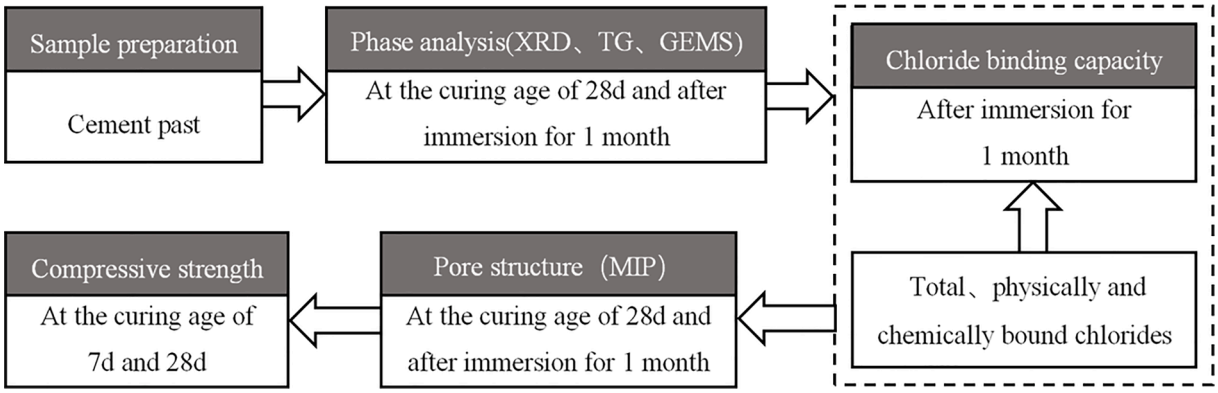

Fig. 1. Experimental process applied in this study.

content of Friedel's salt can be calculated by integrating the dihydroxylation temperature range for the loss of six molecules of main layers water, so as to quantify the content of chemically bound chloride. The calculation method is shown in Formula (2), and the calculation of physically bound chloride content is shown in Formula (3).

$$m_{c.c} = 1000 \cdot \frac{2M_{Cl}}{6 \cdot M_{H_2O}} \cdot m_{loss} = \frac{1000 \cdot m_{loss} \cdot M_{Cl}}{3 \cdot M_{H_2O}} \tag{2}$$

$$m_{c.p} = m_c - m_{c.c} \tag{3}$$

where, $m_{c.c}$ is the amount of chemically bound chloride, mg/g; M_{H2O} is the molar mass of water, g/mol; m_{loss} is the mass loss of six molecules of main layers water of Fs on DTG curves for chloride-exposed sample (260 °C~380 °C in this case), g; $m_{c.p}$ is the amount of physically bound chloride, mg/g.

The compressive strength tests were carried out similar to the China standard GB/T 17671-1999). Cubic samples with size of 40 mm × 40 mm × 40 mm were prepared and tested at the ages of 7 and 28 days respectively. The strength value for each sample was obtained from an average of three specimens.

The pore structure before and after exposed to chloride attack was obtained by using the mercury intrusion pore measurement (MIP), with continuous pressurization from vacuum to 33,000 psia, the measured pore size range is from 5 to 800000 nm.

Thermodynamic modelling was applied to predict the equilibrated hydrate assemblage and exposure solution compositions by using Gibbs free energy minimization software GEMS 3.7 and the recently published cement database CEMDATA 18.01. The database of alkali activated materials was selected in the simulation process, which includes the solid solution model CNASH_ss of C-(N-)A-S-H and the model MaAl-OH-LDH_ss of Mg-Al layered double hydroxide [35,36]. The extended Debye-Hückel equation (Formula 4) with Truesdell-Jones form was adopted for the aqueous phase models [37], which is used to calculate the ion activity coefficients. An ideal gas equation of state was adopted for the gaseous phase models [38,39].

$$\log_{10}\gamma_j = \frac{-A_\gamma z_j^2 \sqrt{I}}{1 + aB_\gamma \sqrt{I}} + b_\gamma I + Log_{10}\frac{x_{jw}}{X_w} \tag{4}$$

where γ_j and z_j are the activity coefficient of aqueous species j respectively. A and B are electeostatic parameters, I is the ionic strength of the aqueous electrolyte phase, x_{jw} is molar quantity of water, and X_w is the total molar amount of the aqueous phase, a and b are the average ion size.

3. Results and discussion

3.1. Phase composition

3.1.1. XRD analysis

Fig. 2 illustrates the XRD patterns of all mixtures before and after immersed in chloride solutions. Fig. 2(a) shows that before in contact with chloride, the main hydration products of ordinary Portland cement are C-S-H type gels, $Ca(OH)_2$ (CH, PDF# 76-0571) and ettringite (Et, PDF# 41-1451). Limited amount of calcite (*Cc*, PDF# 05-0586) and Monocarbonate (Mc, PDF# 41-0727) are also detected, implying a certain degree of carbonation. The diffraction of Quartz (Q, PDF# 46-1045) is observed in the reference mix, probably due to the impurities in Portland cement. In terms of alkali activated mixtures, the main reaction product is a C-S-H (I) type gels, this type of gels present a obviously higher peak intensity and crystallinity when compared to the C-S-H gels in Portland cement systems. It should be noticed that the presence of AFm type phases such as strätlingite in the reaction product of alkali activated slag is frequently reported from previous studies [40–43], however AFm type phases formed in alkali activated materials are usually poorly crystalline and therefore difficult to be observed from the XRD patterns. Monocarbonate is also presented in all alkali activated samples, indicating a certain degree of carbonation. When $Ca(OH)_2$ and γ-Al_2O_3 are added to partly replace slag, a clear diffraction peak of $Ca(OH)_2$ is presented within the reaction products, and its peak intensity is qualitatively related to the $Ca(OH)_2$ contents that added. Besides the presence of CH, no additional diffraction peaks are observed, it means that in terms of the well crystallized phases, the incorporation of γ-Al_2O_3, or the $Ca(OH)_2$ to γ-Al_2O_3 ratio shows an limited influence on the phase composition, and the chemical reaction between $Ca(OH)_2$ and other starting materials is not obvious.

The XRD patterns of all samples immersed in chloride solution for one month are presented in Fig. 2(b). For Portland cement based samples, the most obvious phase change is the presence of Freidel's salt (Fs, PDF# 42-0558), this is due to the chemical reactions between available calcium, alumina phases in pore solution and free chlorides, as have mentioned in many previous studies [29,44–46]. For the alkali activated mixes without calcium and alumina addition (sample S0), the diffraction of Freidel's salt is observed as well, but with obviously lower peak intensity compared to the case of Portland cement, it may indicate that the reference alkali activated slag sample has a lower amount of chemically bound chloride. Regarding the alkali activated mixtures with $Ca(OH)_2$ and γ-Al_2O_3 addition, it is interesting to observe that the CH diffraction peaks shown before chloride immersion are no longer significant, only a weak and even ignorable CH diffraction peak can be found in samples with 14 % CH addition (SCA1), indicating that CH probably participated in the generation of Fs [47]. The Fs diffraction peak is observed in all cases, and qualitatively speaking, there is a detectable difference of Fs content in samples with different $Ca(OH)_2$ and γ-Al_2O_3 contents,

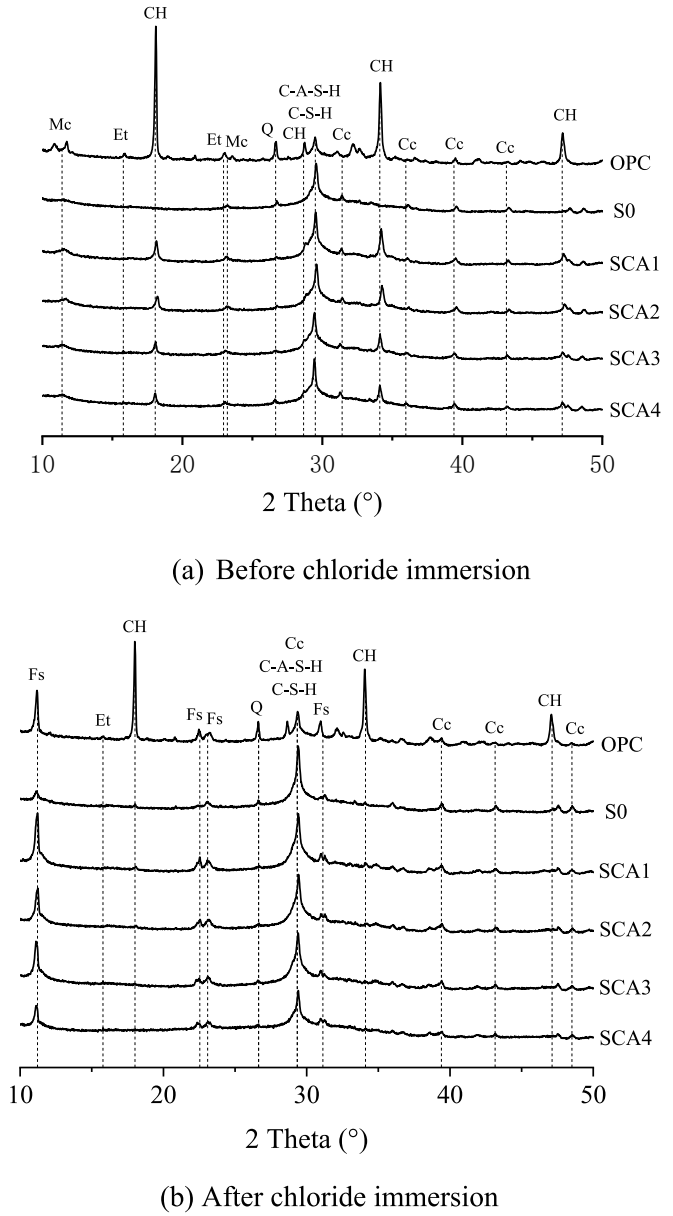

Fig. 2. XRD patterns of mixtures before and after immersed in chloride solution.

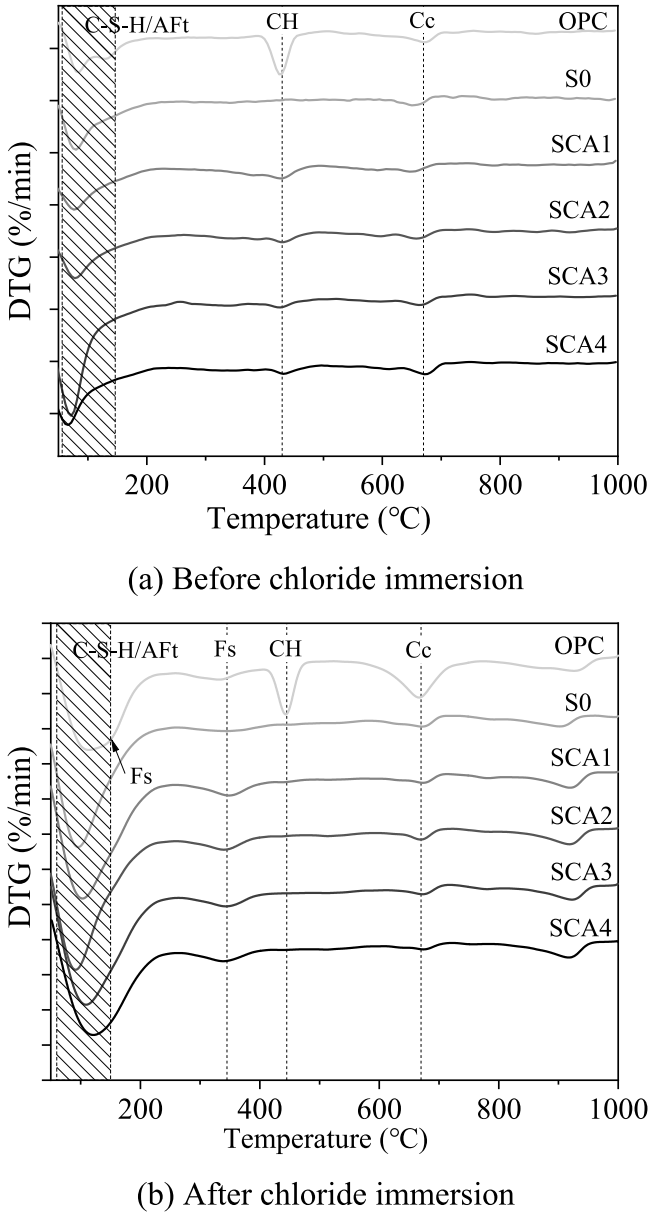

Fig. 3. DTG curves of mixtures before and after immersed in chloride solution.

demonstrating that adding calcium and alumina phases exhibits a positive effect on chloride binding of alkali activated slag, and the Ca/Al ratio of the binder is indeed an factor that affecting the chloride binding capacity. In addition, the diffraction peak of Mc is not obvious in mixes after chloride immersion, probably because of the peak overlapping. But it is more likely that the Mc (CO_3-AFm) also transformed into Fs in presence of chloride, similar phenomenon was also found in a previous study [48].

3.1.2. DTG analysis

Fig. 3 shows the DTG curves of all mixtures before and after chloride immersion. As can be seen from Fig. 3(a) that the hydrated OPC samples show four typical mass losses between 50 °C and 1000 °C, the one between around 50 °C and 100 °C is mainly assigned to the decomposition of free water within the hydrated matrix [49], a slight shoulder at about 130 °C is generally considered as the mass loss of ettringite [50]. The mass losses at around 430 °C and 660 °C refer to the decomposition of Ca$(OH)_2$ and $CaCO_3$, respectively [51,52]. Alkali activated slag mixtures show a slight difference regarding the mass loss characteristics compared to Portland cement, the reference mix (S0) presents only two typical DTG curves, attributing to the release of free and gel water within the temperature range of 50 °C and 100 °C, and the decomposition of $CaCO_3$ at around 650 °C and 700 °C, respectively. Based on the XRD and DTG analysis, it can be referred that both calcite (Cc) and Monocarbonate (Mc) contribute to the mass loss of $CaCO_3$ in all samples. In accordance with the XRD patterns, Ca$(OH)_2$ is also identified from the DTG analysis, demonstrating that the partial replacement of slag binder by Ca$(OH)_2$ and γ-Al_2O_3 results in the presence of residual Ca$(OH)_2$ within the reacted products, which proves again that the additionally provided Ca$(OH)_2$ is not fully reacted in the modified alkali binding system. It is also worth noticing that the mixtures with a higher γ-Al_2O_3 and lower Ca$(OH)_2$ contents exhibits a relatively higher mass loss of $CaCO_3$, which may referring a higher amount of Mc within the reaction products (assuming all mixes are having the same degree of carbonation).

Fig. 3(b) depicts the DTG curves of mixes after immersed in chloride solution, all samples show a typical mass loss between around 260 °C

and 380 °C, demonstrating the presence of Freidel's salt and therefore chemically bound chloride within the hardened matrix [53]. Well related with the XRD results, the decomposition of $Ca(OH)_2$ is only significant in Portland cement based mixes, and its mass loss in alkali activated materials can be ignored based on the DTG result, which suggest that all remaining $Ca(OH)_2$ before immersion are participated into chemical reactions, forming Fs and perhaps other non-crystalline phases. In terms of the mass losses between about 50 °C and 200 °C, there is a difference on the DTG peak width and decomposition temperature range among cement and alkali activated samples, this can be attributed to the different amounts of Fs formed in each mixture, and its loss of 4 molecular water at around 180 °C, resulting in an overlapping of Fs and gel water mass loss peaks [47,54,55]. It is possible that the structure changes of the reacted gels due to $Ca(OH)_2$ and γ-Al_2O_3 addition also play a role on the mass loss characters within this temperature range. The analysis of XRD together with DTG verifies that providing additional calcium and alumina containing phases in the starting material helps to promote the formation of Fs within the reaction products after exposed to chloride solution, which may indicate a better chloride binding capacity of the binder.

3.2. Chloride binding capacity

The total, physically and chemically bound chlorides of all mixtures after exposed to chloride solution are summarized in Fig. 4. The total bound chloride content in Portland cement based samples after 1 month of immersion is 13.64 mg/g, which is obviously higher than that in the reference alkali activated mix (S0, 11.92 mg/g), proofing again that Portland cement system possesses a higher chloride binding capacity than alkali activated materials in general [56,57]. When calcium and alumina containing phases are added in alkali activated materials to partly replace the binder, a remarkable increase on the total bound chloride content is presented. The total bound chloride is increased by 31.7 %, 42.3 %, 37.1 %, and 22.9 % respectively, when the $Ca(OH)_2$ to γ-Al_2O_3 mass ratios shift from 14/1 to 8/7, showing that after phase modification, the alkali activated samples are able to exhibit a comparable or better chloride binding capacity when compared to Portland cement mixtures. An optimum bound chloride content is presented in mixtures with a $Ca(OH)_2$ content of 3 % and γ-Al_2O_3 content of 12 %, which shows again that the initial Ca/Al ratios in the starting material is an important factor of chloride binding capacity, this result is in consistent with previous researches on the chloride binding behaviors in both cement and alkali activated systems [27]. As for the type of bound

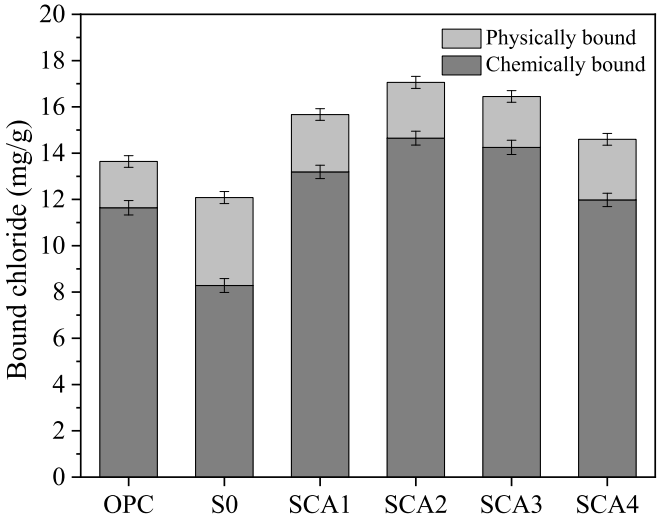

Fig. 4. Total, physically and chemically bound chloride contents of all mixtures.

chlorides, the chemically bound one accounts for around 85.3 % of the total bound chlorides in Portland cement samples. Similar to Portland cement, the chemical binding is also the dominate chloride binding form in alkali activated materials. The addition of Ca and Al mainly results in the increment of chemically bound chloride, together with the phase composition analyze shown in Section 3.1, it can be concluded that the increased chemically bound chloride is owing to the formation of Fs within the reaction products. The physically bound chloride seem to be less affected by the Ca and Al addition. However theoretically, slag replacement by $Ca(OH)_2$ and γ-Al_2O_3 would results in a reduced absolute slag dosage in the starting material, therefore less formed C-S-H gels and eventually decreased ability to physically bound chloride. Considering the fact that after chloride attack, the CH is disappeared from XRD patterns, it is possible that those CH participated in the formation of additional gels, or modifies the chemical composition of the reacted gels, contributing to the physical binding of chloride. Besides, the nano sized γ-Al_2O_3 particles may also contribute to the physical binding. The limited shifts of physically bound chloride content is suggested to be the combined effect of the above factors. Overall, adding Ca and Al phases in the initial binder is an effective approach of improving the total chloride binding ability of alkali activated slag. Besides, it should be noticed that the formation of Mg-Al LDHs are usually identified in the reaction products of alkali activated slag, which also present the ability of chloride binding. But a recent study indicated that in case of alkali activated materials, the chloride adsorbed by Mg-Al LDH surface accounts for 90 % of the total chloride binding content, while the chemically bound chloride is only 10 % [24]. Therefore it is suggested that further research on the role of LDH in AAM is still necessary. While in this study, the only precursor of Mg-Al LDHs is slag, and its content is fixed for each recipe, thus the differences in properties of AAS is caused by the addition of Ca and Al phases, and the property comparison between each recipe is then practical.

3.3. Pore characteristics

The porosity and pore size distribution of all mixes before and after immersed in chloride solution are presented in Fig. 5 and Table 3, respectively. Fig. 5 shows that the Portland cement based sample show a total porosity of 30.17 % after 28d of curing, while this value is 12.47 % for alkali activated mix without calcium and alumina replacement. This result is in accordance with previous researches that alkali activated materials usually exhibits a more condensed matrix when compared to Portland cement [56,58]. A denser matrix may also indicates that alkali activated materials possess a better resistance to ion transportation than Portland cement. When calcium and alumina containing phases are introduced in the system, there is a increase of porosity in general, when the $Ca(OH)_2$/γ-Al_2O_3 contents shift from 14 % / 1 % to 8 % / 7 %, the porosity is increased by 29.0 %, 16.0 %, 10.1 % and 1.2 %, respectively. The increased porosity is probably due to the $Ca(OH)_2$ addition, the excess $Ca(OH)_2$ accelerates the hydration and condensation of alkali activated slag, thus resulting in more macro pores [28]. Meanwhile, the nano sized Al_2O_3 seems to compensate the negative effect of $Ca(OH)_2$. After immersed in chloride solution for one month, all mixtures show a decrease of porosity, based on the results from Section 3.1, it is highly possible that the reduced porosity is assigned to the obviously decreased $Ca(OH)_2$ content and the formation of Fs within the reaction products.

It can be seem from the pore size distribution characters listed in Table 3 that the Portland cement samples show a obviously different pore size distributions compared to alkali activated materials. The much higher porosity of cement based mixes is mainly located in the pore size range that smaller than 200 nm, especially between 20 and 200 nm (referring to the harmful pores). For the harmless pores with the size less than 20 nm, the cement based mixes show an more or less three times higher porosity than alkali activated materials, while among the alkali activated samples, porosity within this size range seems to be independent of chemical composition of the starting material. And regarding the

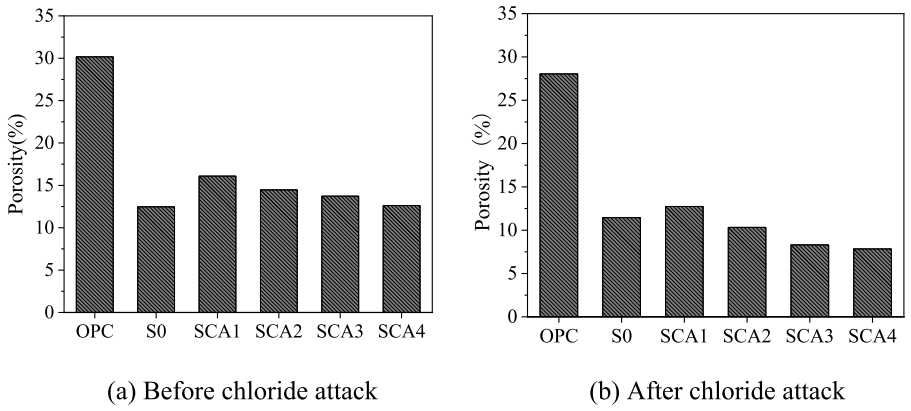

Fig. 5. Porosity of mixtures before and after chloride attack.

Table 3
Pore size distributions of mixtures before and after chloride attack (porosity, %).

Condition	Sample ID	<20 nm	20 ~ 50 nm	50 ~ 200 nm	>200 nm	Total
Before immersion	OPC	7.78	5.11	7.05	10.22	30.17
	S0	2.43	0.29	0.39	9.36	12.47
	SCA1	2.42	0.41	0.60	12.66	16.09
	SCA2	2.35	0.33	0.56	11.23	14.47
	SCA3	2.43	0.36	0.58	10.36	13.73
	SCA4	2.43	0.38	0.48	9.33	12.62
After immersion	OPC	6.03	4.74	10.32	6.95	28.04
	S0	3.77	0.29	0.33	7.06	11.45
	SCA1	3.59	0.37	0.57	8.21	12.74
	SCA2	3.07	0.27	0.37	6.61	10.32
	SCA3	3.28	0.25	0.34	4.43	8.30
	SCA4	3.24	0.25	0.24	4.11	7.84

harmful pores that bigger than 200 nm, the porosity of all mixes are at a similar level, regardless of binder type. However, the chemical composition of alkali activated materials seem to affect the porosity in this size range, follow the tendency that the higher of the $Ca(OH)_2$ / γ-Al_2O_3 ratio, the higher of the porosity. After immersed in chloride solution, the reduced porosity of cement based samples seems mainly due to the pore refinement from higher than 200 nm to 50–200 nm, slight reduction of porosity is also shown in the pore range of less than 50 nm. The alkali activated samples show a slight increase of harmless pores that smaller than 20 nm, and a relatively obviously reduction of porosity for pores larger than 200 nm. The effect of $Ca(OH)_2$ / γ-Al_2O_3 ratio on porosity shares the same tendency with the mixes before chloride attack. The results may suggest that the chloride binding behavior promotes the pore refinement to some extent, especially for the pores with a size higher than 200 nm, and this effect is influenced by the binder type and binder chemical composition.

3.4. Compressive strength

The potential influence of $Ca(OH)_2$ and γ-Al_2O_3 on compressive strength of alkali activated slag is evaluated and shown in Fig. 6. The reference alkali activated mixture show a 7/28 d compressive strength of 48.2 MPa/62.8 MPa, which are obviously higher than the Portland

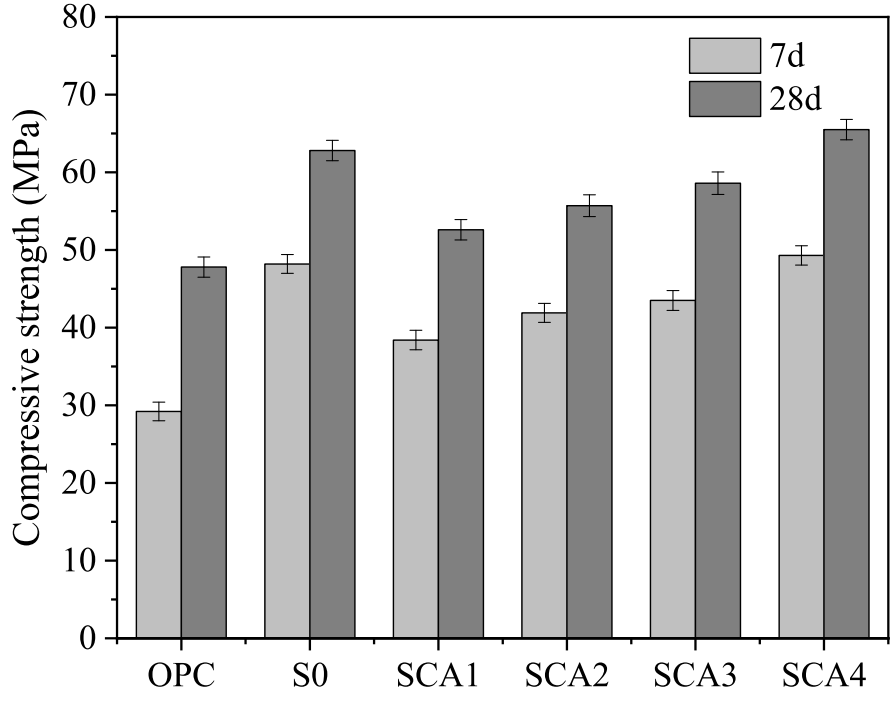

Fig. 6. Compressive strength of mixtures after 7 and 28 days of curing.

cement based samples under the same binder content and water to binder ratio. The porosity results shown in Section 3.4 can be an explanation for the strength difference of these two types of binder, namely the higher the porosity, the lower of the strength. Alkali activated materials also presents a much higher 7 d compressive strength than Portland cement. When replaced by 14 % of CH and 1 % of NA, the 28 d compressive strength of alkali activated sample is reduced by 16.2 % (to 52.6 MPa), According to XRD and TG results, this probably due to the large amount of unreacted CH within the reaction products, which is loosely accumulate in the pores and not tightly connected with the material matrix [59]. As the NA content increases from 1 % to 7 %, there is a gradual increase of 28 d compressive strength from 52.6 MPa to 65.5 MPa, eventually showing a very similar strength compared to the reference alkali activated slag mixture, this is related to the effect of nano size NA on pore structure refinement. From the MIP results, it can be seen that the addition of NA leads to the trend of pore refinement. The strength results imply that the addition of $Ca(OH)_2$ and γ-Al_2O_3 obviously affect the mechanical properties of alkali activated materials, the $Ca(OH)_2$ presents an negative effect while the γ-Al_2O_3 shows a positive influence in general. In addition, porosity results of alkali activated materials can be regarded as an indication of the strength changes, especially for the pores with the pore size larger than 200 nm. As can be seem from Table 3 and Fig. 6 that the strength results are well related with the amount of pores that larger than 200 nm. Therefore, it is suggested that from the physical aspect, the addition of $Ca(OH)_2$ and nano γ-Al_2O_3 affect the compressive strength by increasing / decreasing the total amount of harmful pores within the hydrated matrix. As for the early stage strength, the 7 d compressive strength of alkali activated material reaches 76.8 % of its 28d strength, much higher than the case of Portland cement (61.1 %). The influence of $Ca(OH)_2$ and γ-Al_2O_3 incorporation on this issue seem to be limited, showing a value between around 73.0 % and 75.3 %.

3.5. GEMS modelling

Following the testing method mentioned in Section 2.3, the modelled phase composition of alkali activated slag with different $Ca(OH)_2$ and γ-Al_2O_3 replacements before and after chloride attack are illustrated in Fig. 7. The input reaction degree of the original slag is assumed and fixed at 46 %, based on the previous experiences of the authors; the amount of unreacted CH content is calculated based on the thermal analysis results of this study, and used as input values. As shown in Fig. 7(a), the main reaction products of the reference mixture (S0) are C-A-S-H type gels, Mg-Al LDH, Strätlingite and AFm-OH, in accordance with the modelling work of Provis [48]. When 15 % of slag is replaced by $Ca(OH)_2$ and γ-Al_2O_3, there is an reduction of the C-A-S-H gel content in general, this can be attributed to the reduced amount of available slag and the formation of calcium enriched phases of AFm and Strätlingite. The amount of Mg-Al LDH is mainly controlled by the slag content, because slag is the only origin of Mg and the system is able to provide sufficient Al. $Ca(OH)_2$ and γ-Al_2O_3 addition promotes the formation of AFm family (Strätlingite and AFm-OH in this case) in general, which verifies the hypothesis proposed in this study that Fs precursors' formation and content can be tailored by adjusting the initial mix proportions (especially calcium and alumina content) in alkali activated slag system. Fig. 7(a) also implies again that with a fixed slag replacement level, the $Ca(OH)_2$/γ-Al_2O_3 ratio is an important factor that affecting the phase composition, and therefore other key performances of the modified alkali activated slag system. A higher AFm-OH content is preferred under the condition of relatively high $Ca(OH)_2$/γ-Al_2O_3 ratios, while relatively low $Ca(OH)_2$/γ-Al_2O_3 contents favor the formation of Strätlingite.

After immersed in chloride solution, as shown in Fig. 7(b), all mixture show the formation of Friedel's salt, this is consistent with the results of XRD and DTG. Fs formation is at the expense of AFm family, and also CH for mixtures with Ca and Al phase modification. The modelled Fs content is closely related to the $Ca(OH)_2$/γ-Al_2O_3 ratios in the system, and there may exist a optimum $Ca(OH)_2$/γ-Al_2O_3 dosage in terms of the chloride binding capacity, this result matches the measured chemically bound chlorides content in Section 3.2 in general. It should be noted that the modelling results indicate that the chloride binding behavior show a influence on the absolute solid content in a unit volume, namely the formation of Fs decreases the total porosity of the matrix, this result in well related with the MIP tests presented in Section 3.3. The reduced porosity may also indicate a increased resistance to chloride transport from the physical aspect, again, the $Ca(OH)_2$/γ-Al_2O_3 ratio play an important role on this issue. It worth of noticing that the thermodynamic modelling helps to present a general view on how Ca and Al minerals affect the phase composition of alkali activated slag before and after chloride attack, further modifications such as boundary settings and experimental validations are still necessary for this newly established binding system.

4. Conclusions

This paper investigates the feasibility of improving the chloride binding capacity of alkali activated slag by introducing calcium and aluminate containing phases as partial binder replacements. The effect of $Ca(OH)_2$ and nano γ-Al_2O_3 contents, chloride immersion on phase composition, amount and type of bound chloride, pore size distribution and mechanical properties of alkali activated slag are evaluated and discussed. The following conclusions can be drawn based on the results:

The addition of $Ca(OH)_2$ together with γ-Al_2O_3 results in the formation of additional AFm-OH, Strätlingite and CH within the reaction products, which are able to form extra Friedel's salt in the matrix when exposed to chloride solution.

The chloride binding capacity of alkali activated slag can be improved by incorporating $Ca(OH)_2$ and γ-Al_2O_3 phases into the system, the enhanced chloride binding capacity is mainly contributed by the

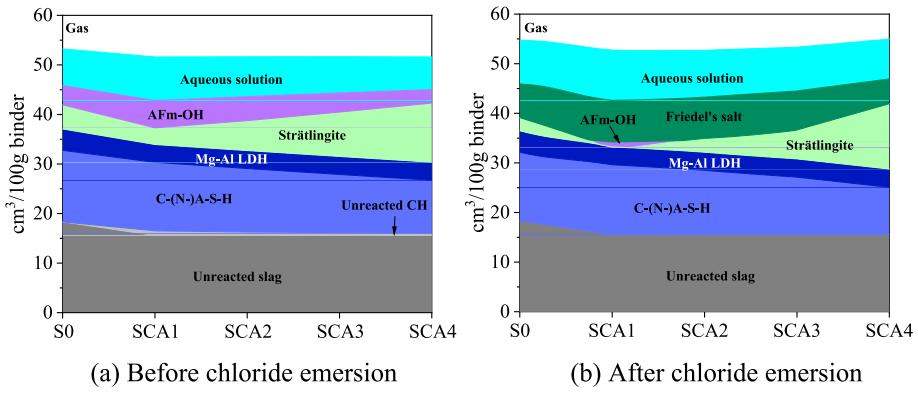

Fig. 7. Thermodynamic modelling on the phase assemblages before and after chloride emersion.

chemically binding of chloride via Fs precursors. The $Ca(OH)_2$ / γ-Al_2O_3 ratio is an important factor regarding this property.

Alkali activated slag exhibits a distinguish pore size distribution and obviously lower porosity when compared to cement based binder, the addition of $Ca(OH)_2$ slightly increases the porosity while γ-Al_2O_3 shows a contrary effect. The chloride binding behavior condensed the matrix to some extent, mainly by refining the pores with the sizes larger than 200 nm.

The compressive strength of alkali activated binder is related to the amount of pores that larger than 200 nm, the higher the porosity, the lower the compressive strength. The 7 d and 28 d compressive strengths of alkali-activated slag are much higher than OPC. The addition of CH has a negative impact on the compressive strength, and NA incorporation is able to compensate the negative impact of CH.

The GEMS simulation results are consistent with the experimental results in this study, the addition of calcium and aluminum containing phases promotes the formation of AFm family, and therefore generates more Friedel's after chloride immersion, exhibiting a better chlorine binding ability.

CRediT authorship contribution statement

Tingli Yang: Writing – original draft, Investigation, Data curation. **Xiaochun Fan:** Methodology, Investigation. **Xu Gao:** Writing – review & editing, Supervision. **Qian Gu:** Writing – review & editing, Conceptualization. **Shi Xu:** Validation, Writing – review & editing. **Zhonghe Shui:** Methodology, Validation.

Declaration of Competing Interest

The authors declare that they have no known competing financial interests or personal relationships that could have appeared to influence the work reported in this paper.

Data availability

Data will be made available on request.

Acknowledgements

The authors acknowledge the financial supports of "National Nature Science Foundation of China (No.52108244)", "Fundamental Research Funds for the Central Universities (WUT:2022jc-07-01)"and Knowledge Innovation of Wuhan-Shuguang Project (No. 20220108010201 92).

References

[1] F. Puertas, B. González-Fonteboa, I. González-Taboada, et al., Alkali-activated slag concrete: Fresh and hardened behaviour, Cem. Concr. Compos. 85 (2018) 22–31.
[2] C. Shi, A.F. Jiménez, A. Palomo, New cements for the 21st century: the pursuit of an alternative to Portland cement, Cem. Concr. Res. 41 (7) (2011) 750–763.
[3] M.C.G. Juenger, F. Winnefeld, J.L. Provis, et al., Advances in alternative cementitious binders, Cem. Concr. Res. 41 (12) (2011) 1232–1243.
[4] N.K. Lee, H.K. Lee, Reactivity and reaction products of alkali-activated, fly ash/slag paste, Constr. Build. Mater. 81 (2015) 303–312.
[5] F. Ameri, P. Shoaei, S.A. Zareei, et al., Geopolymers vs. alkali-activated materials (AAMs): A comparative study on durability, microstructure, and resistance to elevated temperatures of lightweight mortars, Constr. Build. Mater. 222 (2019) 49–63.
[6] J.L. Provis, Alkali-activated materials, Cem. Concr. Res. 114 (2018) 40–48.
[7] M. Grutzeck, S. Kwan, M. DiCola, Zeolite formation in alkali-activated cementitious systems, Cem. Concr. Res. 34 (6) (2004) 949–955.
[8] A. Wang, Y.i. Zheng, Z. Zhang, et al., The durability of alkali-activated materials in comparison with ordinary Portland cements and concretes: a review, Engineering 6 (6) (2020) 695–706.
[9] M. Babaee, A. Castel, Water vapor sorption isotherms, pore structure, and moisture transport characteristics of alkali-activated and Portland cement-based binders, Cem. Concr. Res. 113 (2018) 99–120.
[10] H. Zhu, Z. Zhang, Y. Zhu, et al., Durability of alkali-activated fly ash concrete: chloride penetration in pastes and mortars, Constr. Build. Mater. 65 (2014) 51–59.
[11] H. El-Didamony, A.A. Amer, H. Abd Ela-ziz, Properties and durability of alkali-activated slag pastes immersed in sea water, Ceram. Int. 38 (5) (2012) 3773–3780.
[12] J. Zuquan, Z. Xia, Z. Tiejun, et al., Chloride ions transportation behavior and binding capacity of concrete exposed to different marine corrosion zones, Constr. Build. Mater. 177 (2018) 170–183.
[13] D. Ravikumar, N. Neithalath, An electrical impedance investigation into the chloride ion transport resistance of alkali silicate powder activated slag concretes, Cem. Concr. Compos. 44 (2013) 58–68.
[14] D.M. Roy, W. Jiang, M.R. Silsbee, Chloride diffusion in ordinary, blended, and alkali-activated cement pastes and its relation to other properties, Cem. Concr. Res. 30 (12) (2000) 1879–1884.
[15] X. Hu, C. Shi, Z. Shi, et al., Compressive strength, pore structure and chloride transport properties of alkali-activated slag/fly ash mortars, Cem. Concr. Compos. 104 (2019), 103392.
[16] J. Fan, H. Zhu, J. Shi, et al., Influence of slag content on the bond strength, chloride penetration resistance, and interface phase evolution of concrete repaired with alkali activated slag/fly ash, Constr. Build. Mater. 263 (2020), 120639.
[17] P.S. Mangat, O.O. Ojedokun, Bound chloride ingress in alkali activated concrete, Constr. Build. Mater. 212 (2019) 375–387.
[18] Y. Wang, Z. Shui, X. Gao, et al., Chloride binding behaviors of metakaolin-lime hydrated blends: influence of gypsum and atmospheric carbonation, Constr. Build. Mater. 201 (2019) 380–390.
[19] Y. Jun, S. Yoon, J.E. Oh, A comparison study for chloride-binding capacity between alkali-activated fly ash and slag in the use of seawater, Appl. Sci. 7 (10) (2017) 971.
[20] Z. Shi, M.R. Geiker, B. Lothenbach, et al., Friedel's salt profiles from thermogravimetric analysis and thermodynamic modelling of Portland cement-based mortars exposed to sodium chloride solution, Cem. Concr. Compos. 78 (2017) 73–83.
[21] M. Gbozee, K. Zheng, F. He, et al., The influence of aluminum from metakaolin on chemical binding of chloride ions in hydrated cement pastes, Appl. Clay Sci. 158 (2018) 186–194.
[22] P. Chen, B. Ma, H. Tan, et al., Effects of amorphous aluminum hydroxide on chloride immobilization in cement-based materials, Constr. Build. Mater. 231 (2020), 117171.
[23] Z. Yang, S. Sui, L. Wang, et al., Improving the chloride binding capacity of cement paste by adding nano-Al2O3: the cases of blended cement pastes, Constr. Build. Mater. 232 (2020), 117219.
[24] X. Ke, S.A. Bernal, J.L. Provis, Uptake of chloride and carbonate by Mg-Al and Ca-Al layered double hydroxides in simulated pore solutions of alkali-activated slag cement, Cem. Concr. Res. 100 (2017) 1–13.
[25] J. Zhang, C. Shi, Z. Zhang, Chloride binding of alkali-activated slag/fly ash cements, Constr. Build. Mater. 226 (2019) 21–31.
[26] P.S. Mangat, O.O. Ojedokun, Free and bound chloride relationships affecting reinforcement cover in alkali activated concrete, Cem. Concr. Compos. 112 (2020), 103692.
[27] H. Zibara, R.D. Hooton, M.D.A. Thomas, et al., Influence of the C/S and C/A ratios of hydration products on the chloride ion binding capacity of lime-SF and lime-MK mixtures, Cem. Concr. Res. 38 (3) (2008) 422–426.
[28] X. Zhu, D. Tang, K. Yang, et al., Effect of $Ca(OH)_2$ on shrinkage characteristics and microstructures of alkali-activated slag concrete, Constr. Build. Mater. 175 (2018) 467–482.
[29] M.V.A. Florea, H.J.H. Brouwers, Chloride binding related to hydration products Part I: Ordinary Portland Cement, Cem. Concr. Res. 42 (2) (2012) 282–290.
[30] X. Gao, Q.L. Yu, H.J.H. Brouwers, Reaction kinetics, gel character and strength of ambient temperature cured alkali activated slag–fly ash blends, Constr. Build. Mater. 80 (2015) 105–115.
[31] X. Gao, Q.L. Yu, H.J.H. Brouwers, Properties of alkali activated slag–fly ash blends with limestone addition, Cem. Concr. Compos. 59 (2015) 119–128.
[32] R. Wang, J. Yu, S. Gu, et al., Effect of ion chelator on hydration process of Portland cement, Constr. Build. Mater. 259 (2020), 119727.
[33] B. Lu, C. Shi, J. Zhang, et al., Effects of carbonated hardened cement paste powder on hydration and microstructure of Portland cement, Constr. Build. Mater. 186 (2018) 699–708.
[34] T. Luping, L. Nilsson, Chloride binding capacity and binding isotherms of OPC pastes and mortars, Cem. Concr. Res. 23 (2) (1993) 247–253.
[35] R.J. Myers, S.A. Bernal, J.L. Provis, A thermodynamic model for C-(N-)A-S-H gel CNASH_ss. Derivation and validation, Cem. Concr. Res. 66 (2014) 27–47.
[36] X. Ke, S.A. Bernal, J.L. Provis, et al., Thermodynamic modelling of phase evolution in alkali-activated slag cements exposed to carbon dioxide, Cem. Concr. Res. 136 (2020), 106158.
[37] D.A. Kulik, T. Wagner, S.V. Dmytrieva, et al., GEM-Selektor geochemical modeling package: revised algorithm and GEMS3K numerical kernel for coupled simulation codes, Comput. Geosci. 17 (2012) 1–24.
[38] R.J. Myers, S.A. Bernal, J.L. Provis, Phase diagrams for alkali-activated slag binders, Cem. Concr. Res. 95 (2017) 30–38.
[39] H. Ye, L. Huang, Z. Chen, Influence of activator composition on the chloride binding capacity of alkali-activated slag, Cem. Concr. Compos. 104 (2019), 103368.
[40] Y. Lin, D. Xu, X. Zhao, Effect of soda residue addition and its chemical composition on physical properties and hydration products of soda residue-activated slag cementitious materials, Materials 13 (7) (2020) 1789.
[41] O.R. Ogirigbo, L. Black, Chloride binding and diffusion in slag blends: influence of slag composition and temperature, Constr. Build. Mater. 149 (2017) 816–825.
[42] M.V.A. Florea, H.J.H. Brouwers, Modelling of chloride binding related to hydration products in slag-blended cements, Constr. Build. Mater. 64 (2014) 421–430.

[43] T. Zhang, W. Tian, Y. Guo, et al., The volumetric stability, chloride binding capacity and stability of the Portland cement-GBFS pastes: an approach from the viewpoint of hydration products, Constr. Build. Mater. 205 (2019) 357–367.
[44] Y. Cao, L. Guo, B. Chen, et al., Thermodynamic modelling and experimental investigation on chloride binding in cement exposed to chloride and chloride-sulfate solution, Constr. Build. Mater. 246 (2020), 118398.
[45] C. Shi, X. Hu, X. Wang, et al., Effects of chloride ion binding on microstructure of cement pastes, J. Mater. Civ. Eng. 29 (1) (2017).
[46] Q. Yuan, C. Shi, G. De Schutter, et al., Chloride binding of cement-based materials subjected to external chloride environment – a review, Constr. Build. Mater. 23 (1) (2009) 1–13.
[47] Y. Wang, Z. Shui, X. Gao, et al., Understanding the chloride binding and diffusion behaviors of marine concrete based on Portland limestone cement-alumina enriched Pozzolans, Constr. Build. Mater. 198 (2019) 207–217.
[48] S. Mundra, D.P. Prentice, S.A. Bernal, et al., Modelling chloride transport in alkali-activated slags, Cem. Concr. Res. 130 (2020), 106011.
[49] I. Ismail, S.A. Bernal, J.L. Provis, et al., Drying-induced changes in the structure of alkali-activated pastes, J. Mater. Sci. 48 (9) (2013) 3566–3577.
[50] Z. Shi, M.R. Geiker, K. De Weerdt, et al., Role of calcium on chloride binding in hydrated Portland cement–metakaolin–limestone blends, Cem. Concr. Res. 95 (2017) 205–216.
[51] A.F. Abdalqader, F. Jin, A. Al-Tabbaa, Development of greener alkali-activated cement: utilisation of sodium carbonate for activating slag and fly ash mixtures, J. Cleaner Prod. 113 (2016) 66–75.
[52] A. Bouaziz, R. Hamzaoui, S. Guessasma, et al., Efficiency of high energy over conventional milling of granulated blast furnace slag powder to improve mechanical performance of slag cement paste, Powder Technol. 308 (2017) 37–46.
[53] J.O. Ukpata, P.A.M. Basheer, L. Black, Slag hydration and chloride binding in slag cements exposed to a combined chloride-sulphate solution, Constr. Build. Mater. 195 (2019) 238–248.
[54] A. Dousti, J.J. Beaudoin, M. Shekarchi, Chloride binding in hydrated MK, SF and natural zeolite-lime mixtures, Constr. Build. Mater. 154 (2017) 1035–1047.
[55] F. Puertas, S. Martínez-Ramírez, S. Alonso, et al., Alkali-activated fly ash/slag cement strength behaviour and hydration products, Cem. Concr. Res. 30 (10) (2000) 1625–1632.
[56] J. Zhang, C. Shi, Z. Zhang, et al., Durability of alkali-activated materials in aggressive environments: a review on recent studies, Constr. Build. Mater. 152 (2017) 598–613.
[57] A.R. Brough, M. Holloway, J. Sykes, et al., Sodium silicate-based alkali-activated slag mortars Part II. The retarding effect of additions of sodium chloride or malic acid, Cem. Concr. Res. 30 (9) (2000) 1375–1379.
[58] B. Akturk, A.B. Kizilkanat, Improvement of durability and drying shrinkage of sodium carbonate activated slag through the incorporation of calcium hydroxide and sodium hydroxide, Constr. Build. Mater. 243 (2020), 118260.
[59] D. Tang, C. Yang, X. Li, Mitigation of efflorescence of alkali-activated slag mortars by incorporating calcium hydroxide, Constr. Build. Mater. 298 (2021), 123873.